nature chemistry

SUPPLEMENTARY INFORMATION

DOI: 10.1038/NCHEM.2723

In the format provided by the authors and unedited.

One-thousand-fold enhancement of high field liquid nuclear magnetic resonance signals at room temperature

Guoquan Liu[1†]*, Marcel Levien[2], Niels Karschin[2], Giacomo Parigi[3], Claudio Luchinat[3], Marina Bennati[1,2]*

[1]Electron-Spin Resonance Spectroscopy, Max Planck Institute for Biophysical Chemistry, Am Fassberg 11, 37077 Göttingen, Germany.

[2]Department of Chemistry, Georg-August-University, Tammannstr. 4, 37077 Göttingen, Germany.

[3]Magnetic Resonance Center (CERM) and Department of Chemistry, University of Florence, Via Luigi Sacconi 6, 50019, Sesto Fiorentino, Italy.

[†] Present address: State Key Laboratory of Natural and Biomimetic Drugs, School of Pharmaceutical Sciences, Peking University, 38 Xueyuan Road, Beijing 100191, China.

*Correspondence to: guoquanliu@bjmu.edu.cn; marina.bennati@mpibpc.mpg.de.

Content

Section 1: Experimental details for ^{13}C-NMR DNP experiments at 94 GHz (ν_{EPR}) /3.4 Tesla/36 MHz (ν_{NMR}). Samples were inserted into EPR capillaries with inner diameter (ID) ranging from 0.2 mm to 0.7 mm, and were degassed by freeze-pump-thaw (1-2) cycles that efficiently removes O_2 and affords T_{1e} close or longer than 300 ns. DNP experiments were performed with a Bruker ElexSys E680 EPR spectrometer equipped with a Bruker AVANCE III 400 MHz NMR console. A Bruker cylindrical resonator EN600-1021H with matched ENDOR coils for ^{13}C NMR at ~36 MHz was employed. For DNP, a liquid sample in a capillary was continuously irradiated by MW usually in resonance with the low-field hyperfine EPR transitions of ^{15}N-TEMPONE (Fig. 1 in the main text) and the nuclear magnetization was subsequently measured with a one-pulse FID detection. For Boltzmann signal, the MW was switched off. To avoid heating of the resonator, a constant flow of N_2 gas was introduced to the cavity.

Section 2: Evaluation of DNP enhancement. DNP enhancements were quantified by comparison of the NMR signal with MW irradiation to the Boltzmann signal without MW. NMR spectra were obtained by Fourier transformation of the NMR FID. The line width was usually large (~10 ppm) due to the inhomogeneity of our magnet that is designed for EPR purpose and not optimized for NMR experiments. The DNP enhancement is generally calculated by:

$$\varepsilon = \frac{I_{\mathrm{DNP}}}{I_{\mathrm{Bolt}}} * \frac{n_{\mathrm{Bolt}}}{n_{\mathrm{DNP}}} \qquad (1a)$$

where I_{DNP} and $I_{\mathrm{Bolt.}}$ are the integrated area of the DNP and Boltzmann ^{13}C signal under identical conditions, respectively; n_{DNP} and $n_{\mathrm{Bolt.}}$ are the number of accumulated scans for DNP and Boltzmann measurements, respectively. Usually it is convenient to evaluate enhancements by scaling the spectra to the same noise level. For doing this, the signal and the noise of the same measurement are divided by the square-root of the number of acquired scans. This applies to both the DNP and the Boltzmann signal. After this operation, the noise of the two measurements corresponds to the noise in a single scan. Then from eq. (1a) the DNP enhancement results as:

$$\varepsilon = \frac{I_{\mathrm{DNP,scaled}}}{I_{\mathrm{Bolt,scaled}}} * \frac{\sqrt{n_{\mathrm{Bolt}}}}{\sqrt{n_{\mathrm{DNP}}}} \qquad (1b)$$

For DNP in $^{13}CCl_4$ $^{13}CHCl_3$ and $^{13}CDCl_3$, 1 to 8 scans were usually sufficient to achieve reasonable signal/noise (> ~ 10) and the measurement is repeated for ≥ 3 times. The uncertainty of the DNP signal is usually ~ 5-10 %. For Boltzmann signal, thousands of scans were required. Because of the various sources of possible errors, the uncertainty in the enhancement was evaluated by repeating the experiment with samples under nominally similar conditions. For $^{13}CCl_4$, more than 5 samples with radical concentration from 20 mM to 45 mM have been measured. For $^{13}CHCl_3$, 3 samples with radical concentration of 20 mM (± 5 mM) have been measured. With this procedure, the uncertainty of the enhancement was estimated on the order of ≤ 10 %.

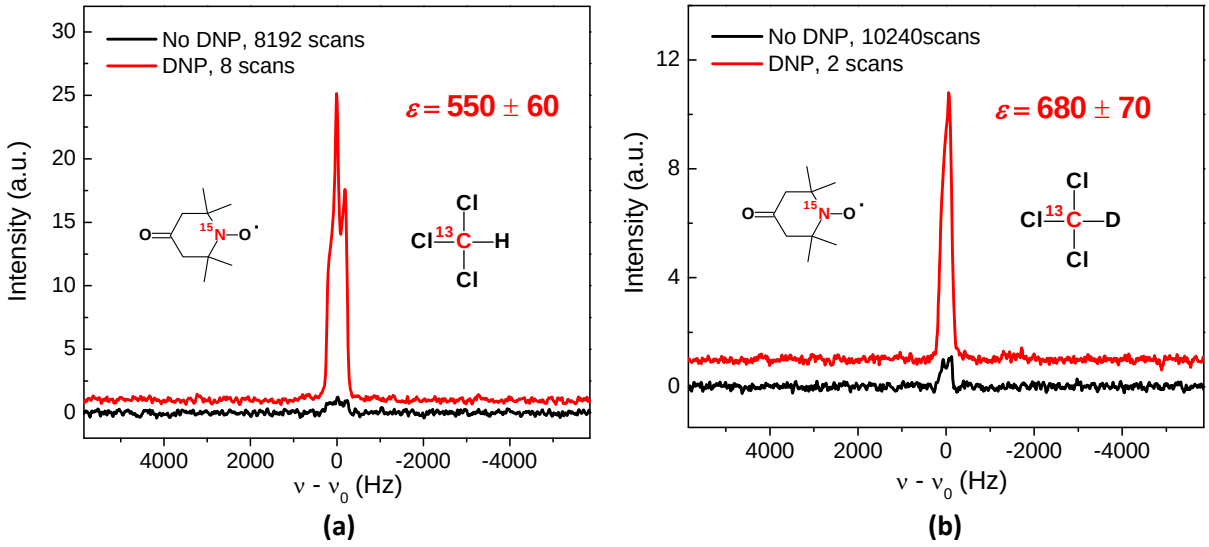

Figure 1 ^{13}C DNP-NMR experiments on $^{13}CHCl_3$ (a) and $^{13}CDCl_3$ (b) doped with 20 mM ^{15}N-TEMPONE at 3.4 Tesla (ν_{EPR} = 94 GHz, ν_{NMR} (^{13}C) = 36 MHz, RT. Black: Boltzmann signal were accumulated with recycle delay of 20 s (~ 4·T_{1n}); Red: DNP with 10 s of MW irradiation (P_{MW} ≤ 150 mW, B_1 ≤ 1.5 G). Sample volume is ~200 nL. Numbers of scans are given in the figure legend. For comparison at the same noise level, DNP and Boltzmann spectra were scaled down by the square-root of the number of respective scans. The enhancements are then obtained by eq.1b.

Section 3: Build-up of DNP enhancements and measurements of T_{1n}

$T_{\text{build up}}$ was obtained from mono-exponential fitting of the DNP-signal build up curve (Supplementary Fig. 2, left). T_{1n} values were used to calculate the leakage factor f ($f = 1 - T_{1n}/T_{1n}^{0}$) and were measured from the decay of the DNP signal back to Boltzmann equilibrium (Supplementary Fig. 2, right). For the latter measurement, a short pumping pulse of 2 s was employed to minimize possible changes in sample temperature. The extracted time constant are summarized in Supplementary Table 2. The diamagnetic $T_{1n,0}$ of ^{13}C was measured to be 30 s for $CHCl_3$ at a ^{1}H 300 MHz NMR spectrometer and it is about 200 s for CCl4 according to a previous report.[1]

$^{13}CCl_4$-30mM

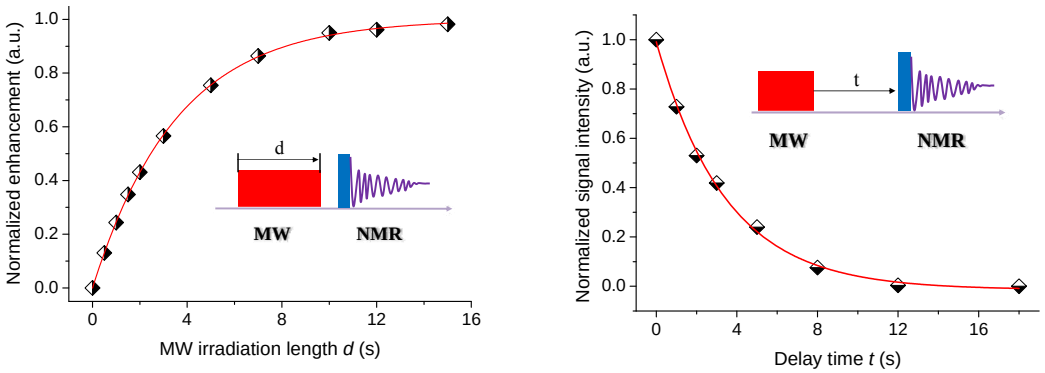

$^{13}CHCl_3$-20mM

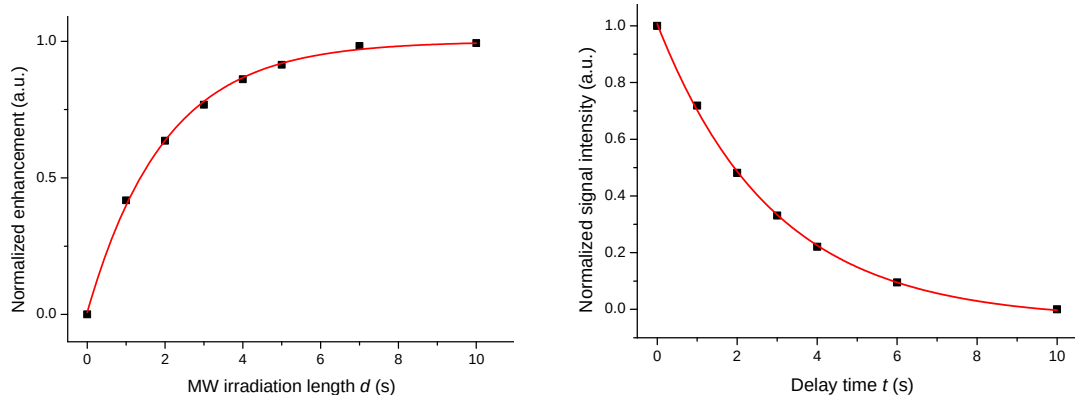

$^{13}CDCl_3$-20mM

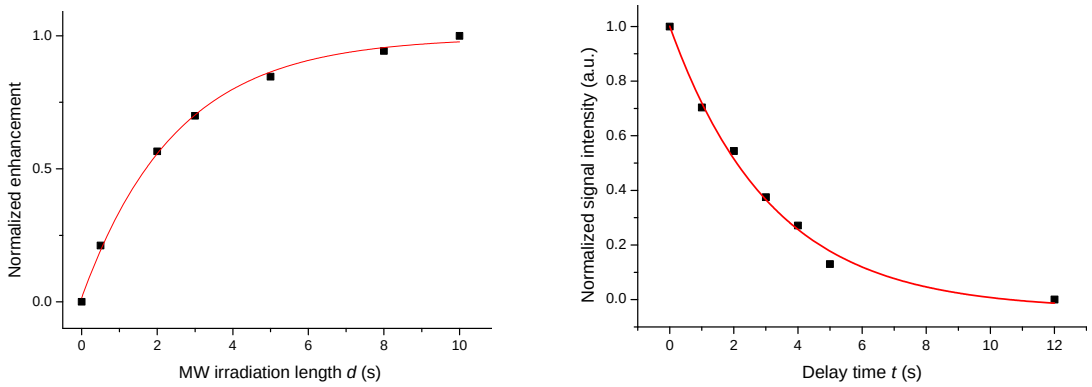

Figure 2 Left side: Build-up of ^{13}C-DNP signal with MW irradiation time. Signal was normalized to the maximal DNP signal. Right side: Signal decay as a function of time after DNP of 2 s MW irradiation.

Section 4: Determination of saturation factors at 94 GHz

In several recent papers we and others pointed out the difficulties of extracting coupling factors from enhancements with nitroxide radicals,[2,3] due to the evaluation of the saturation factor in eq. 1 (main text). However, a few methods based on ELDOR or paramagnetic shifts measurements have been proposed, and we have recently also validated the theoretical descriptions to predict s. The 94 GHz EPR spectrum of the ^{15}N-TEMPONE radical consists of two lines (Fig. 1, inset, main text) arising from the hyperfine splitting of the radical S = ½ coupled to the ^{15}N, I = ½ nuclear spin. The saturation factor s (eq. 1, main text) is the average of the irradiated (s_1) and the other EPR transition (s_2) through $s = (s_1 + s_2)/2$. We measured s_1 via a pre-saturation sequence, in which the saturation pulse is increased until the EPR FID intensity reaches a steady state value (Supplementary Section 4.1). s_2 was determined in a similar experiment (Supplementary Section 4.1) or was predicted by saturation transfer theory (Supplementary Section 4.3). This last step required an independent experimental determination of factors entering the saturation factor s_2, i.e. T_{1e}, T_{2e} and the Heisenberg exchange constant K_x. Internal nitrogen ^{15}N relaxation was neglected under our conditions (see Supplementary Section 4.3). We found that the available MW power at 94 GHz/W-band ($P \leq 250$ mW) is not sufficient for saturating the irradiated EPR line, a situation that is quite different from that at low EPR frequencies (i.e. 9 GHz). At high radical concentrations ($c \geq 20$ mM), and for the solvents used here, this situation leads to a saturation factor $s = s_1 = s_2$ (Supplementary Section 5), within an error of < 5 %. Determination of saturation factors at 94 GHz was conducted in two steps.

Section 4.1. Determination of s_1 and s_2 for ^{15}N-TEMPONE at 94 GHz. 94-GHz electron-electron double resonance (ELDOR)[1] experiments were performed with a Bruker ElexSys E680 EPR spectrometer. Microwave (MW) detection and irradiation were conducted in a single-mode cylindrical resonator with a typical band width of ≤ 60 MHz. The MW pumping frequency was always set at the center of the MW absorption dip. Detection frequency was set either on the same position of the dip (for saturation experiments to determine s_1) or about 60 MHz apart (for ELDOR experiments to determine s_2). To measure the saturation factor of the irradiated EPR line s_1, the intensities of the EPR FID were monitored as a function of the length of the pumping pulse (pumping and detection were at same frequency). For sufficiently long irradiation, the intensity of the EPR FID decreased to a steady state value. s_1 can be calculated as the signal reduction from the normalized equilibrium signal to the steady-state value (Supplementary Fig. 3a). s_2 was measured in a similar way but frequency of the detection pulse was set on the neighbor EPR line and apart from the center of MW dip (ELDOR). s_1 and s_2 were measured for three samples (Table 1, main text), $^{13}CHCl_3$-20mM, $^{13}CDCl_3$-20mM and $^{13}CCl_4$-20mM. We obtained $s_2/s_1 \geq 0.90 \pm 0.05$ in all three samples. For $^{13}CCl_4$-30mM (Table 1, main text), T_{2e} becomes very short and measurement of s_2 becomes difficult. However, the ratio s_2/s_1 is already close to maximum (≈ 1) at 20 mM concentration and should not change at the higher concentration (more details in Supplementary Section 4.3).

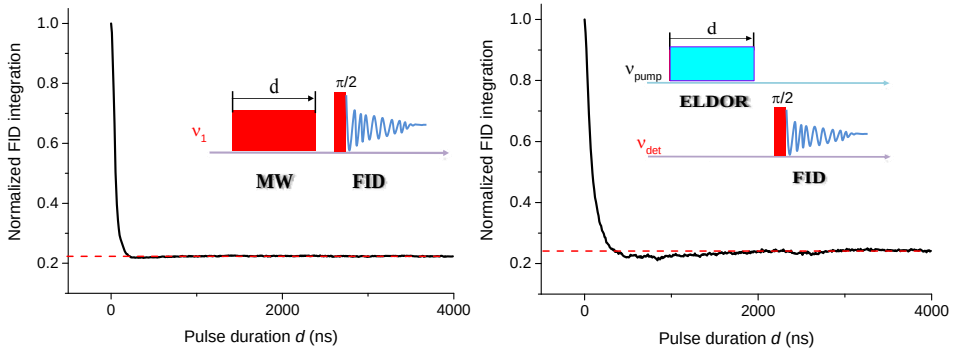

(a) (b)

Figure 3 Experiments to measure s_1 (a) and s_2 (b) at 94 GHz. Inset shows the pulse sequences. Sample ^{13}C-CCl_4 doped with ~20 mM ^{15}N-TEMPONE. FID detection pulse length was 30-50 ns.

Section 4.2. ELDOR experiments with ^{15}N TEMPONE at 9 and 34 GHz to determine the Heisenberg exchange constant K_x.

Saturation transfer ELDOR experiments were performed at a Bruker ElexSys E580 EPR spectrometer that can operate at both X and Q band frequencies (9 and 34 GHz, respectively). A Bruker FlexLine microwave resonator EN4118X-MD-4 was used for X band measurements, and a Bruker ER5106QTW operating at TE_{012} mode for Q band. A MW amplifier TWT-1 KW was used for X band experiments, and for Q band experiments (model 187Ka, Applied System Engineering Inc.). Heisenberg exchange coupling constants K_x were extracted from experiments of polarization recovery EPR (PR-EPR) and polarization recovery ELDOR (PR-ELDOR).[3] The intensities $i_{1,2}$ of the two recovery curves were fitted with the equations

$$i_{1,2} = A_{1,2}e^{-2w_e t} \pm B_{1,2}e^{-(2w_e+2w_n+K_x)t} \qquad (2)$$

using shared parameters. Internal ^{15}N relaxation w_n is assumed to be negligible (see Supplementary Section 4.3). Typical traces and fits at 34 GHz are displayed in Supplementary Fig. 4. The K_x for $CHCl_3$ and CCl_4 were determined to be 2.9±0.8*10^9 s^{-1} M^{-1} and 2.5±0.8*10^9 s^{-1} M^{-1}, respectively.

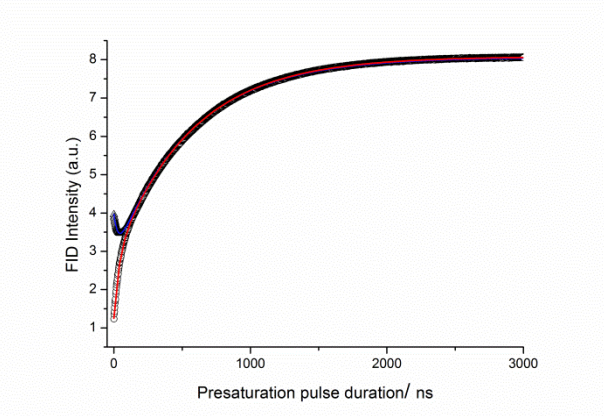

Figure 4 34-GHz experiments to measure the Heisenberg exchange constant K_x. Sample was $CHCl_3$ doped with 10 mM TEMPONE, room temperature. Pre-saturation EPR curve is in red, pre-saturation ELDOR curve in blue.

Table 1 Experimental results from saturation experiments at 9 and 34 GHz. MW field B_1 ~ 3-4 G at both frequencies.

	$CHCl_3$ (10mM, 9 GHz)	$CHCl_3$ (10mM, 34 GHz)	CCl_4 (4mM, 34 GHz)	CCl_4 (20mM, 34 GHz)
T_{1e} (ns)	500±50	560±50	520±50	490±50
T_{2e} (ns)	60±6	46±5	100±10	33±5
s_1 (experimental)	0.95±0.05	0.94±0.05	0.93±0.05	0.90±0.05
s_2 (experimental)	0.84±0.05	0.89±0.05	0.68±0.04	0.82±0.04
s_2/s_1 (experimental)	0.88±0.08	0.94±0.08	0.73±0.08	0.91±0.08
s	0.90±0.05	0.92±0.05	0.81±0.05	0.86±0.08
K_x (s^{-1} M^{-1})	2.7±0.8·10^9	3.0±0.8·10^9	2.5±0.8·10^9	-

Section 4.3. Calculations of s_1 and s_2. The theoretical expressions for s_1 (irradiated) and s_2 for the two-line EPR spectrum of ^{15}N-TEMPONE were reported previously,[3,4] and depend on microwave field strength B_1, T_{2e}, the concentration dependent Heisenberg exchange rate $\omega_{ex} = c \cdot K_x$ as well as the transition probabilities $2w_e = 1/T_{1e}$ and the probability for internal nitrogen relaxation $2w_n$:

$$s_1 = 1 - \frac{w_e(2(w_e+w_n)+\omega_{ex})}{(1/4)\gamma_e^2 B_1^2 T_{2e}(4w_e+2w_n+\omega_{ex})+w_e(2(w_e+w_n)+\omega_{ex})} \qquad (3)$$

$$s_2 / s_1 = 1 - \frac{2}{2+\frac{w_n}{w_e}+\frac{\omega_{ex}}{2w_e}} \qquad (4a)$$

We have previously shown[2,5] that w_n can be neglected with respect to ω_{ex} in solutions of small nitroxide radicals when rotational correlation time is small (for $\tau_c < 60 \pm 20$ ps, $w_n < 10^6$ s^{-1}). ω_{ex} was scaled with temperature according to $\omega_{ex} = nK_x = 8kT/3\eta$, where η is the sample viscosity, n is the sample concentration. At 244 K, ω_{ex} is 4×10^6 s^{-1}, and it is still much larger than w_n. In samples with high radical concentration, where $\frac{\omega_{ex}}{2w_e} \gg 1$, a calculation of s_2 according to eq. 4 leads to $s_2 \approx s_1$. Calculated factors are reported in Supplementary Table 3.

Section 4.4: Comparison with ^{14}N labelled nitroxide. If ^{15}N labelled nitroxide is not available, naturally occurring ^{14}N nitroxide can also be used and the saturation factor scales according to the attainable ELDOR effect among the three hyperfine lines (arising from the hyperfine coupling with a nuclear spin $I = 1$). The theory for saturation transfer for the ^{14}N case was treated in our recent paper, Ref. 2. We reported that, at X-band, highest effective saturation is generally achieved when pumping the central line. In this case, the saturation factors s_1 and s_3 of the neighbor lines were given by the expression:

$$s_1 = s_3 = s_2 \cdot \left(1 - \frac{1}{1 + \frac{1}{6w_e}(3w_n + \omega_{ex})} \right) \qquad (4b)$$

We can use this expression for an estimate of the effective saturation factor for $^{13}CCl_4$ doped with 30 mM ^{14}N-TEMPONE, using the assumption that g-anisotropy at high fields does not affect the ELDOR effect. As the ELDOR effect is not dependent on mw power, we compare the two cases (^{15}N and ^{14}N) assuming that the irradiated line is completely saturated. In this case, eq. 4a delivers an effective saturation factor of $s = (s_1 + s_2)/2 \approx 0.97$ and eq. 4b for the three line case gives $s = (s_1 + s_2 + s_3)/3 \approx 0.94$.At a lower concentration, for instance 5 mM TEMPONE, the ratio $s(^{15}N)/s(^{14}N)$ is about 85 %.

Section 5: Summary of DNP parameters for $^{13}CCl_4$, $^{13}CHCl_3$ and $^{13}CDCl_3$.

Table 2 Summary of DNP parameters in ^{13}C labelled solvents at room temperature. Relative error of T_{1e} and T_{2e} are estimated ~ 10-15%, relative error of s_1, f, T_{1n} and T_{build} is < 5%. B_1 is calculated from s_1 experimental values using eq.3. Absolute error in ξ is estimated ≤ 15 %, however the error in the trend is less.

	Radical concen. (mM)	T_{1n} (s)	$T_{Buildup}$ (s)	s_1	s	B_1 (G)	T_{1e} (ns)	T_{2e} (ns)	f	ε	ξ
$^{13}CCl_4$	30	3.4	3.5	0.75	0.75	1.7	370	18	1	930±100	-0.47
$^{13}CHCl_3$	20	2.9	2.0	0.63	0.63	1.1	410	23	0.9	550±60	-0.37
$^{13}CDCl_3$	20	3.1	2.5	0.70	0.70	1.0	490	29	0.9	680±70	-0.41

Table 3 Saturation factors of ^{15}N-TEMPONE in $^{13}CCl_4$ at 94 GHz and nuclear relaxation time T_{1n} of ^{13}C as a function of temperature and concentrations. Relative error of T_{1e} and T_{2e} are estimated ~ 10-15%, error of s_1 is < 5%, and error of T_{1n} is ~ 5%.

Concentration (mM)	Temperature (K)	T_{1e} (ns)	T_{2e} (ns)	s_1	s_2/s_1 (cal.)	s (cal.)	T_{1n} (s)
5	297	380	77	0.90	0.66	0.75	22
	263	540	80	0.94	0.63	0.77	15
	253	670	74	0.95	0.63	0.78	-
	249	650	76	0.96	0.59	0.76	12
	244	780	88	0.97	0.60	0.77	> 35
20	297	280	28	0.8	0.88	0.75	5.30
	263	330	33	0.83	0.84	0.76	2.74
	243	330	40	0.87	0.76	0.77	2.13
35	297	180	16	0.81	0.89	0.76	2.75
	263	230	20	0.8	0.87	0.75	1.60
	243	220	27	0.81	0.79	0.72	1.10
45	297	310	12	0.83	0.95	0.81	2.16
	263	310	16	0.84	0.92	0.81	1.15

Section 6: Evaluation of scalar relaxation rate

The Overhauser equation can be written in the form of transition probabilities,[6]

$$\varepsilon \approx -\xi \cdot f \cdot s \cdot \left|\frac{\gamma_s}{\gamma_I}\right| = -\frac{w_2 - w_0}{w_0 + 2w_1 + w_2} \cdot \frac{w_0 + 2w_1 + w_2}{w_0 + 2w_1 + w_2 + R_{1dia}} \cdot s \cdot \left|\frac{\gamma_s}{\gamma_I}\right| \qquad (5)$$

Here is $w_0 = w_{0,d} + w_{0,s}$, $w_2 = w_{2,d}$, $w_1 = w_{1,d}$ and the suffices d and s denote the dipolar and scalar contributions, respectively. After abbreviation, we then rewrite eq. 5 as

$$\varepsilon \approx -\frac{w_2-w_0}{w_0+2w_1+w_2+R_{1dia}} \cdot s \cdot \left|\frac{\gamma_S}{\gamma_I}\right| \qquad (5.a)$$

The sum of all nuclear transition probabilities in eq. 5.a relates to T_{1n} by

$$T_{1n} = \frac{1}{w_0+2w_1+w_2+R_{1dia}} \qquad (6)$$

Inserting eq.6 into eq. 5.a leads to:

$$\frac{\varepsilon}{s \cdot T_{1n}} \approx -(w_2 - w_0) \cdot \left|\frac{\gamma_S}{\gamma_I}\right| \qquad (7)$$

At W band, the dipolar contributions to w_0 , as well as to w_2 , have strongly decayed because dipolar correlation functions have dispersions characterized by correlation times of molecular motion on the order of tens of ps. Thus, any remaining contribution is expected only from scalar relaxation $w_{0,s}$. For this high field case, eq. 7 can be simplified to

$$\frac{\varepsilon}{s \cdot T_{1n}} \approx w_{0,s} \cdot \left|\frac{\gamma_S}{\gamma_I}\right| \qquad (8)$$

When the three parameters on the right side (ε, s, T_{1n}) can be experimentally determined, $w_{0,s}$ can be extracted using eq. 8. This applies to samples with 20 mM, 30 mM and 45 mM radical concentration. The calculated $w_{0,s}$ values are shown in Fig. 2 in the main text.

Practically, ε and T_{1n} are difficult to measure in samples with low radical concentrations (e.g. 5 mM), where T_{1n} is long and very long MW irradiation ($3 * T_{1n}$) is required to determine ε. In these cases, the equation for the time evolution of the enhancement can be used. When the time for electron spins to reach a steady state is much shorter than T_{1n}, the enhancement builds up exponentially with T_{1n} [4]

$$\varepsilon(t) \approx -\xi \cdot f \cdot s \cdot \left|\frac{\gamma_S}{\gamma_I}\right| \cdot \left(1 - e^{-t/T_{1n}}\right) \qquad (9)$$

At W band, in the reasonable assumption that $w_{0,d}$ and w_2 can be neglected with respect to $w_{0,s}$, as already described in deriving eq. 8,

$$\varepsilon(t) \approx w_{0,s} \cdot T_{1n} \cdot s \cdot \left|\frac{\gamma_S}{\gamma_I}\right| \cdot \left(1 - e^{-t/T_{1n}}\right) \qquad (10)$$

When t/T_{1n} is close to 0, $1 - e^{-t/T_{1n}} \approx t/T_{1n}$ and thus eq. 10 can be simplified to

$$\varepsilon(t) \approx w_{0,s} \cdot s \cdot \left|\frac{\gamma_S}{\gamma_I}\right| \cdot t \qquad (11)$$

Therefore, with a short MW irradiation time t_0, $w_{0,s}$ can be calculated by,

$$\frac{\varepsilon(t_0)}{s \cdot t_0} \approx w_{0,s} \cdot \left|\frac{\gamma_S}{\gamma_I}\right| \qquad (12)$$

In the 5 mM sample, the order of magnitude of T_{1n} is > 10 s and we applied a MW irradiation time t_0=0.5 s. The calculated $w_{0,s}$ is shown in Fig. 2 in the main text.

Section 7: 94 GHz CW-EPR spectra of ^{15}N-TEMPONE at different temperatures, determination of τ_c

Experimental spectra (red lines) were measured in a degassed sample of ^{13}C-CCl_4 doped with ~5 mM ^{15}N-TEMPONE. "*Easyspin*" simulations [7] (black lines) were used to determine the rotational correlation time τ_c from the EPR line shape at each temperature.

Table 4 Rotational correlation time τ_c obtained from fitting the CW EPR spectra at 94 GHz.

Temperature (K)	297	263	253	249	244
τ_c (ps)	7,7	12,1	15,3	17,4	19,9

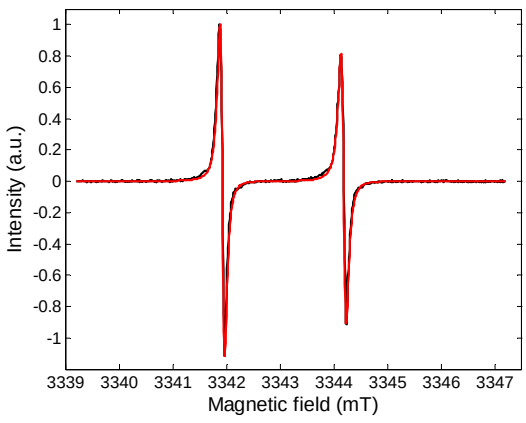

297 K

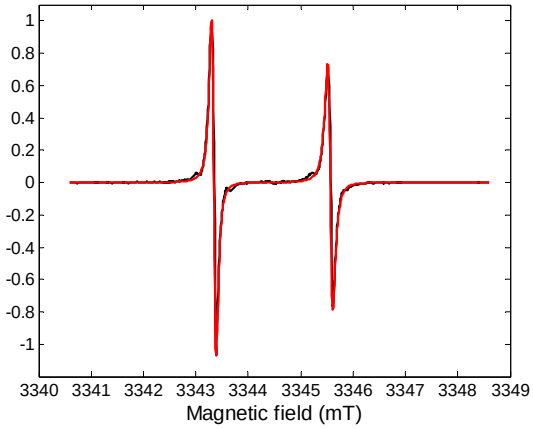

263 K

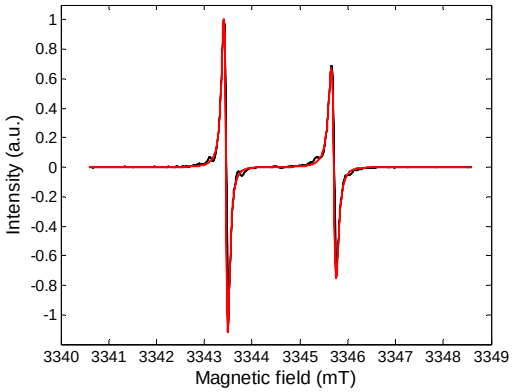

253 K

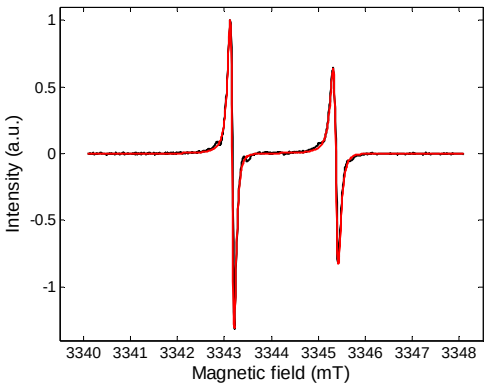

249 K

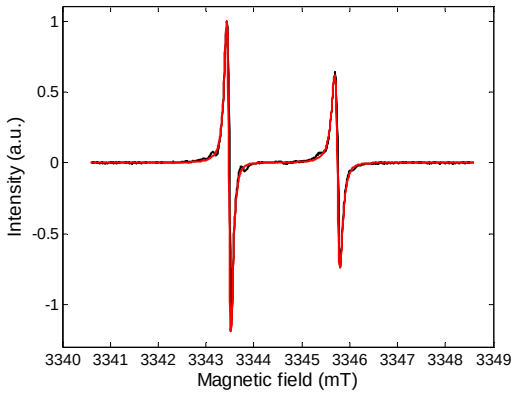

244 K

Figure 5 94 GHz EPR spectra of ^{15}N-TEMPONE at different temperatures and their simulations. Exp. conditions: Microwave power = 0.01581 mW; 0.1 G modulation amplitude, 100 kHz modulation frequency, 1024 points/spectrum.

Section 8: DFT calculations of transient ^{13}C hyperfine interaction. The DFT package Gaussian 09[8] was used for both geometry optimization and single point energy calculation. The geometry optimizations were performed at the B3LYP level of theory using 6-311++G** basis set. The single point energy calculation was performed at B3LYP or BLYP level using 6-311++G(3df,3pd) or EPR-III (only for H N O) basis sets. To calculate the hyperfine coupling constant, a polarization continuum model (PCM) implemented in Gaussian was used to account for the dielectric properties of the solvents.

Table 5 Calculated ^{13}C hyperfine coupling constants by DFT. Unit: MHz Structures **a** and **b** are defined in Supplementary Fig. 6.

	B3LYP/6-311++G(3df,3pd)	B3LYP/ EPR-III	BLYP/ 6-311++G(3df,3pd)	BLYP/ EPR-III
CCl_4	5.48	5.62	14.51	14.89
$CHCl_3$ (**a**)	8.41	8.57	12.59	12.79
$CHCl_3$ (**b**)	3.30	3.39	9.00	9.26

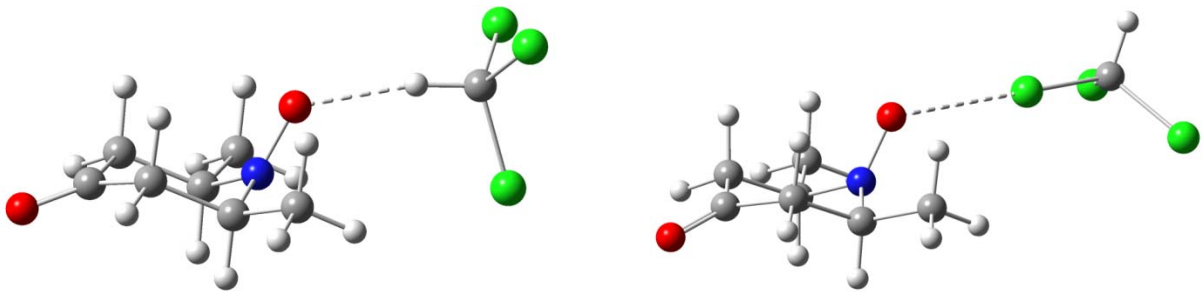

a $d_{O\text{-}H}$= 2.07 Å **b** $d_{O\text{-}Cl}$= 3.03 Å

Figure 6 Two geometry-optimized orientations in TEMPONE-$CHCl_3$. *d* is the distance between the O atom and H/Cl atom (dashed lines). Structure **a** (Supplementary Table 5) is left, structure **b** is right.

XYZ Coordinates of TEMPONE-$CHCl_3$

Orientation a

N	1.30327	0.02184	0.26532
C	2.0784	1.26031	0.51773
C	3.29522	1.27173	-0.44077
C	4.08417	-0.02818	-0.37536
C	3.25158	-1.30112	-0.42902
C	2.03608	-1.23987	0.52921
O	0.41483	0.03294	-0.65702
C	1.12414	-2.45277	0.41603
C	1.20789	2.5022	0.3931
O	5.29145	-0.04822	-0.28268
H	2.44441	1.17255	1.54646
H	3.96481	2.10377	-0.21722
H	2.9192	1.39534	-1.46408
H	3.89262	-2.15333	-0.19784
H	2.87138	-1.42125	-1.4512
H	2.40503	-1.15504	1.55713
H	0.2836	-2.37278	1.10825
H	1.68855	-3.35524	0.66168
H	0.72771	-2.54996	-0.59504
H	1.80286	3.38758	0.6286
H	0.36624	2.45798	1.0872
H	0.81307	2.60201	-0.61832
C	-2.6861	0.00432	-0.14148
H	-1.64728	0.02214	-0.45353
Cl	-3.4586	1.51949	-0.69239
Cl	-3.46479	-1.42425	-0.88201
Cl	-2.7033	-0.11078	1.64802

Orientation b

N	-1.73022	0.09482	0.13744
C	-2.31704	-1.20438	0.56778
C	-3.67188	-1.38996	-0.1738
C	-4.56176	-0.16967	-0.03523
C	-3.90301	1.17052	-0.29962
C	-2.54454	1.30229	0.447
O	-0.95144	0.11511	-0.93239
C	-1.7935	2.58364	0.10539
C	-1.34659	-2.35743	0.34077
O	-5.75648	-0.26177	0.28346
H	-2.51667	-1.09724	1.63752
H	-4.2068	-2.26169	0.19984
H	-3.44937	-1.54986	-1.23447
H	-4.58862	1.96515	-0.0095
H	-3.70119	1.26236	-1.37246
H	-2.733	1.26248	1.52338
H	-0.86198	2.64376	0.66732
H	-2.40781	3.44944	0.35647
H	-1.55009	2.61526	-0.95447
H	-1.79642	-3.29046	0.68307
H	-0.42083	-2.19513	0.89173

H	-1.098	-2.44899	-0.71445
C	3.89866	0.06482	-0.4917
Cl	2.0663	0.07091	-0.6565
Cl	4.51436	-1.55044	0.1787
H	4.32866	0.18876	-1.47102
Cl	4.49081	1.47757	0.5521

Section 9: NMRD data: experimental details and fitting model

Longitudinal relaxation rates at magnetic fields ranging from 0.01 to 40 MHz proton Larmor frequency were measured using the field cycling technique with a high sensitivity Stelar Spinmaster FFC-2000-1T. ^{13}C relaxation rates of $^{13}CCl_4$ and $^{13}CHCl_3$ solutions of 200 mM TEMPONE were measured and normalized to 1 mM radical concentration (Fig. 3 in the main text).

The relaxation profiles show that ^{13}C relaxivity at 40 MHz proton Larmor frequency is more than one order of magnitude smaller than low field relaxivity. This is a clear indication that relaxation at high field is dominated by the contact interaction between the ^{13}C nuclei of the solvents and the unpaired electron of the radical. The dipolar contribution at high fields, in fact, cannot be smaller than about 3/10 of the low field relaxivity for correlation times of few tens of picoseconds or shorter.[6]

Nuclear relaxation rates are provided by the sum of the diffusional and contact contributions (a rotational dipolar contribution could also be possible, the unpaired electron being far from the center of the radical molecule, but it can be neglected in the analysis of the relaxation profile due to the very dominant contact term below 1 T):

$$R_1 = \frac{32}{405}\pi\left(\frac{\mu_0}{4\pi}\right)^2 \frac{1000 N_A M \gamma_I^2 g_e^2 \mu_B^2 S(S+1)}{dD}\left[7J^{tr}(\omega_e) + 3J^{tr}(\omega_I)\right] + \frac{2}{3}S(S+1)J^{con}(\omega_e) \quad (13)$$

where N_A is the Avogadro's constant, M is the molar concentration (in mol dm^{-3}), g_I is the nuclear magnetogyric ratio, μ_B is the Bohr magneton, d is the distance of closest approach between the radical and the solvent molecules, D is the sum of the diffusion coefficients of radical and solvent molecules, ω_e and ω_I are the electron and nuclear Larmor frequencies multiplied by 2π,

$$J^{tr}(\omega) = \frac{1 + 5z/8 + z^2/8}{1 + z + z^2/2 + z^3/6 + 4z^4/81 + z^5/81 + z^6/648} \quad (14)$$

with

$$z = (2\omega\tau_D)^{1/2} \quad (15)$$

and

$$\tau_D = \frac{d^2}{D} \quad (16)$$

According to the pulse diffusion model,[9] the spin density is transferred during random collisions between radical and solvent molecules. By assuming that the stochastic fluctuation modulating the intermolecular contact coupling is described by the Poisson distribution, with τ_p equal to mean time

between collisions (which thus depends on the concentration of the electron spins), the spectral density function for contact relaxation can be described by

$$J^{con}(\omega_e) = \frac{< A^2 >}{\hbar^2} \frac{\pi^2}{\tau_p} \left[\sum_i x_i \tau_i \exp(-\omega_e \tau_i) \right]^2 \qquad (17)$$

where $<A^2>$ is the mean square amplitude of contact coupling constant, τ_i are the contact times between the two molecules, which may vary depending on the points of the molecular collisions, and x_i the relative fractions of encounters.

The NMRD relaxation profiles were thus analyzed using the above model, comprising, in the case of the CCl_4 solvent, the following parameters: d, D, $\sqrt{< (A_{CCl}/h)^2 > \pi^2 / \tau_p}$, x_i and τ_i, with i from 1 to 3. The "average" distance of closest approach d between the C nucleus of CCl_4 and the unpaired electron was fixed to 6 Å (the unpaired electron is not at the center of a spherical molecule, and in our case the distance d can vary between about 4.5 and 10 Å for the many directions along which the solvent molecules approach the paramagnetic complex); the diffusion coefficients D were fixed to 1.7×10^{-9} and 3×10^{-9} m^2/s for TEMPONE in CCl_4 and $CHCl_3$, respectively, at 25 °C.[10,11] Supplementary Table 6 shows the values of the other parameters, providing an excellent agreement with the experimental data (both NMRD profiles and coupling factor). In the case of $CHCl_3$, we assumed that the diffusional and contact contributions are equal to 3/4 of those of $^{13}CCl_4$, with additional contributions arising from the presence of the H nucleus. Therefore, while keeping fixed all previous parameters to the values determined for CCl_4, three additional parameters were included: $\sqrt{< (A_{CH}/h)^2 > \pi^2 / \tau_p}$, describing the contribution to the unpaired electron spin density on the ^{13}C nucleus passed through the H nucleus; τ_{CH}, the contact time between the radical and the H of $CHCl_3$; and r, used to parameterize the additional contribution from translational diffusion arising for the shorter distance of closest approach allowed by $CHCl_3$ with respect to CCl_4 (this further dipolar contribution is calculated through the Solomon equation, with r equal to the electron-proton distance and correlation time equal to τ_{CH}).

Table 6 Best fit parameters obtained from the profiles reported in Fig. 3 (main text) and Supplementary Fig. 7.

	CCl_4		$CHCl_3$	
	25 °C	10 °C	25 °C	10 °C
d (Å)[a]	6.0		6.0[b]	
D (m^2/s)[a]	1.7×10^{-9}	1.4×10^{-9}	3.0×10^{-9}	2.0×10^{-9}
$\sqrt{< (A_{CCl}/h)^2 > \pi^2 / \tau_p}$ ($s^{-3/2}$)	2.6×10^{10}		2.6×10^{10} [b]	
x_i, τ_i (s)	0.001, 8.1×10^{-10}; 0.031, 4.2×10^{-11}; 0.968, 1.1×10^{-12} [c]	9.8×10^{-10}; 5.0×10^{-11}; 1.4×10^{-12}	0.001, 8.1×10^{-10}; 0.031, 4.2×10^{-11}; 0.968, 1.1×10^{-12} [c]	9.8×10^{-10}; 5.0×10^{-11}; 1.4×10^{-12}

$\sqrt{<(A_{CH}/h)^2>\pi^2/\tau_p}$ ($s^{-3/2}$)			8.7×10^9	
τ_{CH} (s)			1.2×10^{-11}	1.5×10^{-11}
r (Å)			3.4[c]	
coupling factor at 3.5 T	-0.47	-0.49	-0.37	-0.37

[a]Values fixed in the best fit procedure of the relaxation profiles.
[b]¾ of the total contribution was considered.
[c]Fixed in order to reproduce the coupling factors at 25 °C.

Table 7 Contributions to the relaxation rates (in s^{-1} mM^{-1}) at 3.5 T and 25 °C, as predicted from parameters reported in Supplementary Table 6.

	$w_{0,d}$, $w_{2,d}$	$w_{1,d}$	$w_{0,s}$	Diffusion	Contact	Dipolar through H	total
CCl_4	1.6E-6, 9.8E-6	0.00227	0.00401	0.00455 (53%)	0.00401 (47%)	-	0.00856
$CHCl_3$	1.7E-5, 1.0E-4	0.00240	0.00301	0.00201 (25%)	0.00301 (38%)	0.00292 (37%)	0.00793

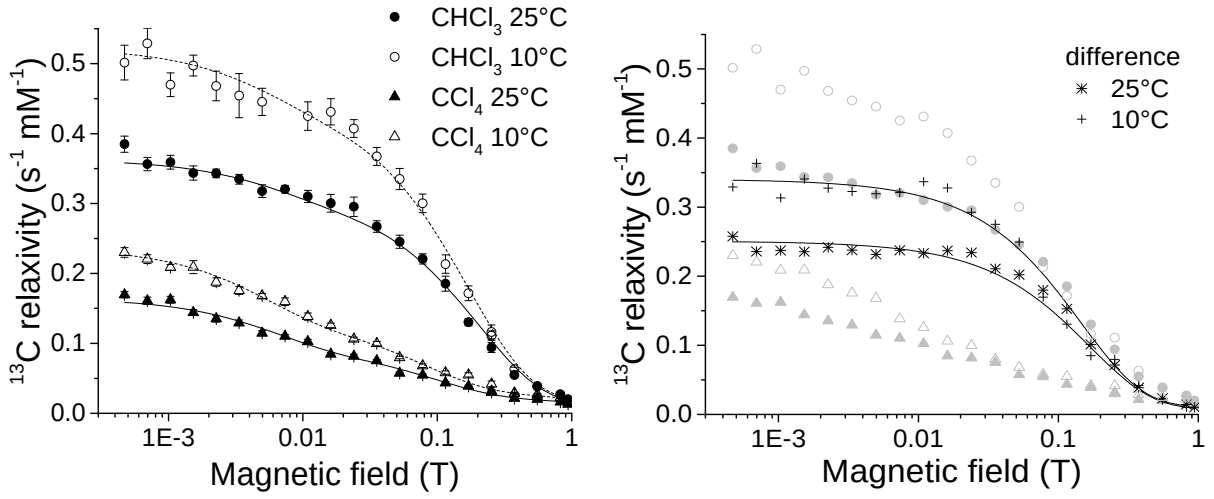

Figure 7 ^{13}C relaxivity of CCl_4 and $CHCl_3$ solutions of 200 mM TEMPONE (best fit profiles are calculated with the parameters reported in Supplementary Table 6). (B) Difference in relaxivity between the profiles acquired for the $CHCl_3$ and the CCl_4 solutions; these profiles should be the relaxivity contribution due to the presence of the H nucleus in chloroform.

References

1. Gillen, K. T., Noggle, J. H. & Leipert, T. K. 13C and 35Cl NMR relaxation in liquid CCl4 - test of extended J-diffusion model for molecular reorientation. *Chem. Phys. Lett.* **17**, 505-509 (1972).
2. Enkin, N. *et al.* A high saturation factor in Overhauser DNP with nitroxide derivatives: the role of 14N nuclear spin relaxation. *Phys. Chem. Chem. Phys.* **17**, 11144-11149 (2015).
3. Türke, M. T. & Bennati, M. Saturation factor of nitroxide radicals in liquid DNP by pulsed ELDOR experiments. *Phys. Chem. Chem. Phys.* **13**, 3630-3633 (2011).
4. Türke, M. T. & Bennati, M. Comparison of Overhauser DNP at 0.34 and 3.4 T with Fremy's Salt. *Appl. Magn. Reson.* **43**, 129-138 (2012).
5. Türke, M. T., Parigi, G., Luchinat, C. & Bennati, M. Overhauser DNP with 15N labelled Fremy's salt at 0.35 Tesla. *Phys. Chem. Chem. Phys.* **14**, 502-510 (2012).
6. Hausser, D. & Stehlik, D. Dynamic nuclear polarization in liquids. *Adv. Magn. Reson.* **3**, 79-139 (1968).
7. Stoll, S. & Schweiger, A. EasySpin, a comprehensive software package for spectral simulation and analysis in EPR. *J. Magn. Reson.* **178**, 42-55 (2006).
8. Gaussian 09, R. D., Frisch, M. J.; Trucks, G. W.; Schlegel, H. B.; Scuseria, G. E.; Robb, M. A.; Cheeseman, J. R.; Scalmani, G.; Barone, V.; Mennucci, B.; Petersson, G. A.; Nakatsuji, H.; Caricato, M.; Li, X.; Hratchian, H. P.; Izmaylov, A. F.; Bloino, J.; Zheng, G.; Sonnenberg, J. L.; Hada, M.; Ehara, M.; Toyota, K.; Fukuda, R.; Hasegawa, J.; Ishida, M.; Nakajima, T.; Honda, Y.; Kitao, O.; Nakai, H.; Vreven, T.; Montgomery, J. A., Jr.; Peralta, J. E.; Ogliaro, F.; Bearpark, M.; Heyd, J. J.; Brothers, E.; Kudin, K. N.; Staroverov, V. N.; Kobayashi, R.; Normand, J.; Raghavachari, K.; Rendell, A.; Burant, J. C.; Iyengar, S. S.; Tomasi, J.; Cossi, M.; Rega, N.; Millam, J. M.; Klene, M.; Knox, J. E.; Cross, J. B.; Bakken, V.; Adamo, C.; Jaramillo, J.; Gomperts, R.; Stratmann, R. E.; Yazyev, O.; Austin, A. J.; Cammi, R.; Pomelli, C.; Ochterski, J. W.; Martin, R. L.; Morokuma, K.; Zakrzewski, V. G.; Voth, G. A.; Salvador, P.; Dannenberg, J. J.; Dapprich, S.; Daniels, A. D.; Farkas, Ö.; Foresman, J. B.; Ortiz, J. V.; Cioslowski, J.; Fox, D. J. Gaussian, Inc., Wallingford CT, 2009.
9. Müller-Warmuth, W., Vilhjalmsson, R., Gerlof, P., Smidt, J. & Trommel, J. Intermolecular interactions of benzene and carbon tetrachloride with selected free radicals in solution as studied by 13C and 1H dynamic nuclear polarization. *Mol. Phys.* **31**, 1055-1067 (1976).
10. Hexem, J. G., Edlund, U. & Levy, G. C. Paramagnetic relaxation reagents as a probe for translational motion of liquids. *J. Chem. Phys.* **64**, 936-941 (1976).
11. Kovacs, H., Kowalewski, J. & Laaksonen, A. Molecular-dynamics simulation of liquid-xixtures of acetonitrile and chloroform. *J. Phys. Chem.* **94**, 7378-7385 (1990).